Design of a 48V electric all-wheel-drive system for a hybrid vehicle

Martin Nell, Daniel Butterweck and Kay Hameyer
Insitute of Electrical Machines (IEM)
RWTH Aachen University
Aachen, Germany
martin.nell@iem.rwth-aachen.de

Orkan Eryilmaz
GKN Driveline
Advanced Driveline Systems Development
Lohmar, Germany
orkan.eryilmaz@gkndriveline.com

***Abstract*—This paper proposes an numerical design-optimization procedure for an $48\,\mathrm{V}$ induction machine implemented in a hybrid vehicle. Based on the scaling laws of the induction machine, the utilization of the equivalent fuel consumption calculation and the Willans approach an Evolutionary Strategy is used to find the optimum induction machine design. The scaling of the induction machine considers axial and radial scaling as well as rewinding. Furthermore, a change of the gear ratio of the hybrid power train is considered. By using a hybrid vehicle model the optimized induction machines are analyzed due to their consumption savings potential. To define the power distribution of the combustion engine and the $48\,\mathrm{V}$ electric machine the equivalent consumption minimization strategy is used.**

***Index Terms*—all-wheel-drive, hybridization, 48V drive, induction machine, numerical optimization, scaling laws**

I. Introduction

An All-Wheel-Drive (AWD) system has approximately $8\,\%$ higher fuel consumption as a comparable front-wheel drive. Besides the reduction of the vehicles weight and the improvement of its aerodynamics the inclusion of a $48\,\mathrm{V}$ electric drive system can reduce the fuel consumption and the local CO_2 emission. Designing a hybrid drive and creating a hybrid strategy cannot be performed separately [1]. On the one hand, the optimum hybrid strategy in a hybrid system is dependent on the vehicles properties, such as weight and the AWD drive train topology, the driving cycle, the gear ratio of the electric drive train and especially the topology, size and power of the hybrid system. On the other hand, the design of the hybrid system is dependent on the hybrid strategy [1]. In this paper a simulation and optimization-based design of an electrical traction unit for a $48\,\mathrm{V}$ AWD hybrid electrical vehicle is presented. The optimization is done for an induction machine (IM) by applying an Evolutionary Strategy and under the utilization of scaling laws for IMs, considering axial and radial geometric scaling of the IM. By using the equivalent fuel consumption calculation [2] in combination with the Willans approach [3] the equivalent consumption for every operating point of the considered IM is calculated. The resulting euqivalent consumptions are used for the objective function of the Evolutionary Strategy. With this procedure the optimum length and radius of the IM, its winding number and the gear ratio of the hybrid power train is calculated. The resulting fuel consumptions by using the optimized machine are simulated by a hybrid vehicle model in Matlab/Simulink.

II. Vehicle Simulation

The hybrid AWD system is modeled by Matlab/Simulink. The model includes different devices of the power train such as the internal combustion engine (ICE), the main gear and the Power Takeoff Unit (PTU). The PTU takes of the power from the front front differential and leads it by the propshaft to the Rear Drive Unit (RDU). The RDU and the hybrid power train are included in the model as well. The different components of the Simulink model are shown in Fig. 1.

A. Controlled AWD Modell in Simulink

The simulation of the vehicle is based on the control scheme shown in Fig. 2. The driving cycle data are used to calculate the actual reference speed v_{ref} of the car. By using (1) - (6) the total driving resistance force F_{Total} is calculated. It is the summation of the air resistance force F_{Air}, the rolling resistance force F_{Rolling}, which depends on the uprising force F_{Uprising} and the lifting force F_{Lifting}, and the slope resistance force F_{Slope}. Here, v_{Car} is the actual velocity of the vehicle, v_{Wind} the wind velocity, c_{w} the drag force coefficient, A the front surface, c_{a} the lift coefficient and m_{Car} the mass of the vehicle, f_{r0}, f_{r1} and f_{r2} the rolling resistance coefficients, ρ_{Air} the density of the air, g the constant of gravitation and β the slope angle.

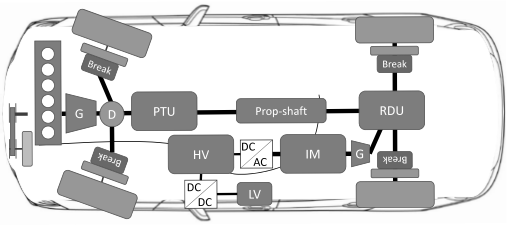

Fig. 1. Components of the simulated vehicle.

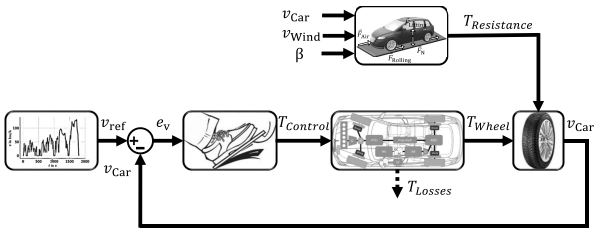

Fig. 2. Control scheme of the vehicle simulation.

$$F_{\mathrm{Air}} = \frac{1}{2} \cdot \left(v_{\mathrm{Car}}^2 + v_{\mathrm{Wind}}^2\right) \cdot c_{\mathrm{w}} \cdot A \cdot \rho_{\mathrm{Air}} \quad (1)$$

$$F_{\mathrm{Rolling}} = \left(f_{r0} + f_{r1} \cdot \frac{v_{\mathrm{Car}}}{100} + f_{r2} \cdot \frac{{v_{\mathrm{Car}}}^4}{100}\right) \cdot F_{\mathrm{Uprising}} \quad (2)$$

$$F_{\mathrm{Uprising}} = m_{\mathrm{Car}} \cdot g \cdot \cos(\beta) - F_{\mathrm{Lifting}} \quad (3)$$

$$F_{\mathrm{Lifting}} = \frac{1}{2} \cdot \left(v_{\mathrm{Car}}^2 + v_{\mathrm{Wind}}^2\right) \cdot c_{\mathrm{a}} \cdot A \cdot \rho_{\mathrm{Air}} \quad (4)$$

$$F_{\mathrm{Slope}} = m_{\mathrm{Car}} \cdot g \cdot \sin(\beta) \quad (5)$$

$$F_{\mathrm{Total}} = F_{\mathrm{Air}} + F_{\mathrm{Rolling}} + F_{\mathrm{Slope}} \quad (6)$$

With the dynamic wheel radius r_{Wheel} the resistance torque $T_{\mathrm{Resistance}}$ is calculated with:

$$T_{\mathrm{Resistance}} = F_{\mathrm{Total}} \cdot r_{Wheel} \quad (7)$$

The driver is simulated by a PI controller. Input e_{v} is the difference of the reference speed v_{ref} and the actual vehicle speed v_{Car}. Its output is the controlled torque demand T_{control}, which for the acceleration case is the necessary ICE torque and for the deceleration case the necessary breaking torque. By applying loss torques due to the losses of the power train devices the driving torques at the wheels T_{Wheel} are calculated. Using the driving torque T_{Wheel} and the resistance torque $T_{\mathrm{Resistance}}$ the actual speed of the vehicle is calculated by

$$v_{\mathrm{Car}} = r_{\mathrm{Wheel}} \cdot \int_0^{\mathrm{t}} \left(\frac{T_{\mathrm{Wheel}} - T_{\mathrm{Resistance}}}{J_{\mathrm{total}}}\right) dt, \quad (8)$$

where J_{total} is the total inertia of the car. The total inertia is the summation of the rotational interia of the wheels J_{Wheel} and translational inertia of the vehicle J_{Car}. The calculation is shown in (10), where m_{Wheel} is the mass of one wheel and e_i a gear dependent mass factor, which represents the rotational part of the mass inertia.

$$J_{\mathrm{Total}} = J_{\mathrm{Wheel}} + J_{\mathrm{Car}} \quad (9)$$

$$= \frac{4}{2} \cdot m_{\mathrm{Wheel}} \cdot r_{\mathrm{Wheel}}^2 + m_{\mathrm{Car}} \cdot e_{\mathrm{i}} \cdot r_{\mathrm{Wheel}}^2 \quad (10)$$

B. Modelling of AWD Devices

The devices of the AWD powertrain, depicted in Fig. 1, are modeled by (11)

$$T_{Input} = \frac{1}{\eta_{diff}} \cdot T_{Output} + T_{Drag}(n), \quad (11)$$

where T_{Input} is the input torque that comes from the engine's side, T_{Output} is the output torque to the wheel's side, η_{diff} the differential efficiency value and $T_{Drag}(n)$ the speed n dependent drag torque of the device. The differential efficiency and the drag torque are determined by test bench measurements. The ICE is modeled by (12), where C_{ICE} is the consumption of the ICE in $\mathrm{l/h}$, ν_{pe} the differential consumption coefficient, P_{Output} the output power of the ICE in kW and $C_0(n)$ the speed dependent no-load consumption of the ICE in $\mathrm{l/h}$.

$$C_{\mathrm{ICE}} = \nu_{pe} \cdot P_{Output} + C_0(n), \quad (12)$$

This type of modeling the AWD power train devices enables the possibility to use the Willans Approach proposed in section III-B.

III. Hybridization

For the design of a hybrid strategy various approaches can be employed. They can be distinguished in rule-based and optimization based methods [4]. In a rule based approach the desired torque distribution of the hybrid system is determined by predefined rules, taking the drivers torque command, the State of Charge (SoC) of the battery and other physical quantities into account [5], [6]. Optimization based methods, e.g. equivalent fuel consumption minimization [2], dynamic programming [7] and fuzzy logic [8], calculate the optimum torque distribution at any time. Therefore, the process of finding the optimum solution is a multi-dimensional optimization problem. In this paper the equivalent fuel consumption minimization strategy is taken into account. The method is used to derive the torque distribution of the ICE and the IM. Its impact is analyzed and compared to results from different driving cycles and hybrid power train topologies. The process of the equivalent fuel consumption calculation is also used for the optimization of the IM.

A. Equivalent Fuel Consumption Minimization

In a hybrid system the battery is discharged during electric driving and can be charged by braking recuperation or by the ICE. In the equivalent fuel consumption minimization strategy the equivalent power and consumption respectively is the power and consumption that is necessary to keep the SoC of the battery fictitious constant. The principle is shown in Fig. 3 and Fig. 4. In the discharge mode the battery is discharged (black power path (a) Fig. 4) and the equivalent fuel consumption is the consumption of the ICE which is necessary to keep the SoC level constant (gray power path (b) Fig. 4). This equivalent fuel consumption is required in a future driving situation to recharge the battery. In the charge mode (black power path (a) Fig. 3) the equivalent fuel consumption is defined as the consumption of the ICE which can be saved (gray power path (b) Fig. 3). This ICE power can be saved in a future situation by using the electric drive. Thereby, the future use of the electric drive can be seperated into a boost mode, where the electric drive supports the ICE and into a pure electric drive.

B. Willans Approach

The Willans approach transforms an efficiency map into a family of functions in an Output-Input-power-plane [3]. The efficiency map is subdivided into equidistant values of the speed. For each value a polynomial Input-Output-power curve (13) can be extracted. With this polynomial functions the hybrid AWD system can be described. A parallel connection of the AWD elements results in an addition of the Willans lines (14) and a series connection in a composition of them (15). In Fig. 4 and Fig. 3 the type of the Willans line connection,

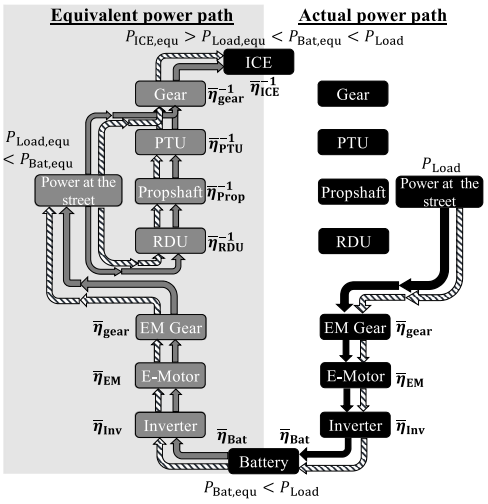

Fig. 3. Equivalent fuel consumption: Charge mode of the battery.

which is either in series or parallel, can be seen by the arrows of the shaded black power path.

$$P_{\text{Input}}(P_{\text{Output}}) = a_x \cdot P_{\text{Output}}^x + ... + a_0 \cdot P_{\text{Output}}^0 \quad (13)$$

$$P_{\text{parallel}}(P_{\text{Output}}) = P_{\text{Input},1}(P_{\text{Output}}) + P_{\text{Input},2}(P_{\text{Output}}) \quad (14)$$

$$P_{\text{serial}}(P_{\text{Output}}) = P_{\text{Input},2}(P_{\text{Input},1}(P_{\text{Output}})) \quad (15)$$

With an interconnection of the Willans lines of the different AWD power train devices, such as the RDU and PTU, a Willans line for the whole AWD power train is achieved. This procedure is executed for the pure AWD system without considering the hybrid power train, for the discharge mode, depicted in Fig. 4, and for the charge mode depicted in Fig. 3. The connection of the devices is done along the shaded black power path (Path (c) in Fig. 4 and Fig. 3, that describes the calculation path for the equivalent consumption calculation using the Willans Approach, and ends at the ICE. With this definition the power at the street, also called load power P_{load}, is defined as the output power of the Willans approach P_{Output}.

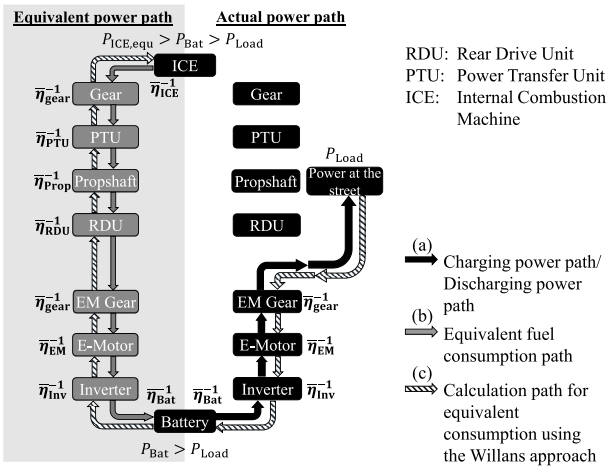

Fig. 4. Equivalent fuel consumption: Discharge mode of the battery.

The input power P_{Input} describes the necessary power of the ICE for the non-hybrid, the discharge and the charge mode. Because of the fact, that the speed of the main gear and the ICE is dependent on the main gear's ratio the Willans lines are calculated for each gear. The resulting Willans curves of all three modes for gear three are shown in Fig. 5. For the calculation of the equivalent consumption in the charge mode a future pure electric mode is taken into account. With this approach it is possible immediately to see the consumption and equivalent consumptions of the ICE for each operating point. This approach will be used to configure the objective function of the design optimization of an IM.

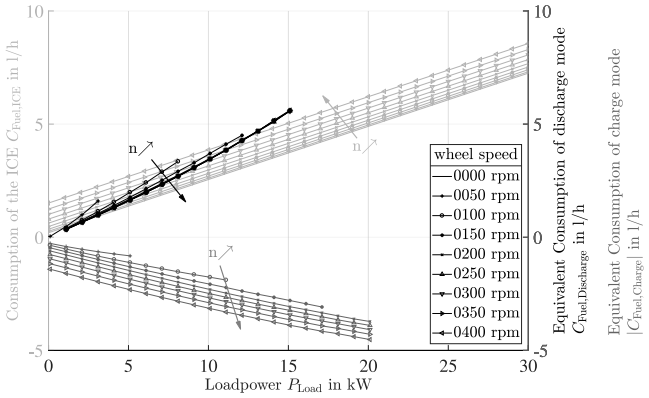

Fig. 5. Willans lines of the pure AWD, the discharge and the charge mode.

IV. Induction Machine Simulation

The simulation of an IM by the finite-element-method (FEM) takes a large number of simulation time steps to build up the machines rotor flux matrix [9]. Therefore, the use of the FEM in a mathematical optimization procedure is not suitable due to time-consuming calculations. A proposed hybrid simulation approach for IMs 2D-finite-element (FE) calculating of Von Pfingsten, Nell and Hameyer [9], [10] drastically decreases the simulation time by shortening the transient build-up of the rotor flux. Nevertheless, this hybrid approach is still not sufficient for the application in a mathematical optimization procedure. To overcome the time-consuming calculations of the FEM scaling laws of the induction machine are used. Scaling laws are a popular method in physics and engineering and are often used in numerous examples. Žarko, Stipetič and Ramakrishnan published several papers about the scaling laws for synchronous machines (SM). In [11] and [12] the procedures of radial and axial geometrical scaling and of rewinding for a SM are introduced. In [13] and [14] the scalable SM models are used to find the optimum sizing of a SM traction motor. For the IM Žarko presented a method to design premium efficiency IM using scaling laws for its equivalent circuit parameters in [15]. Bone's research in [16] deals with the influence of the rotor diameter and length on the rating of IMs.

A. Scaling Procedure

The basis of the scaling procedure of the IM are the FEM solutions in a I_1-f_2-map of a reference IM, which is calculated by the hybrid simulation approach of von Pfingsten, Nell and Hameyer [9], [10], where I_1 is the stator current vector and f_2 rotor frequency vector. Without changing the field solution of the IM the FE-solutions are scaled in the I_1-f_2. By taken into account the inverter requirements maximal current and maximal dc-link voltage and the operation strategy Minimum-Torque-Per-Electrical-Losses (MTPEL) the I_1-f_2-maps are transformed into torque-speed-operation maps (T-n-map). In the transformation into the T-n-map the motor as well as the generator operation mode are considered.

1) Geometric Scaling: For the geometric scaling of the IM the radial scaling factor $\mathrm{k_r}$ and the axial scaling factor $\mathrm{k_a}$ is introduced. The length l of the IM are scaled by (16), the surfaces A by (17) and the volume by (18)

$$l^{'} = l \cdot \mathrm{k_a} \tag{16}$$

$$A^{'} = A \cdot \mathrm{k_r k_a} \tag{17}$$

$$V^{'} = V \cdot \mathrm{k_r^2 k_a} \tag{18}$$

According to Bone's [17] a time scaling factor k_{t1} has to be used to satisfy that the magnetic flux density B is kept constant. This time scaling factor is equal the scare of the radial scaling factor. Fig. 6 shows a change of the rotor resistance R_2^2 has an influence on the current distribution of the stator and rotor currents I_1 and I_2^2 respectively. Therefore, a change of the rotor resistance R_2^2 due to a geometrical scaling of the IM has to be considered in the time scaling factor to keep the field distribution constant. Fig. 6 also illustrates the impact of the time scaling factor $\mathrm{k_t}$. By scaling the inductances with the inverse of $\mathrm{k_t}$ the current distribution and therefore the field distribution is kept constant.

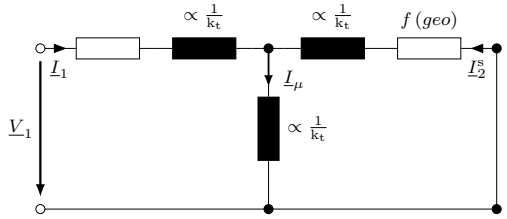

Fig. 6. Scaling factor dependencies of the elements of the equivalent circuit diagram of a squirrel cage induction machine.

The additional time scaling factor $\mathrm{k_{t2}}$ due to the change of the rotor bar geometry is

$$\mathrm{k_{t2}} = \frac{1}{\mathrm{k_{R1}}} \tag{19}$$

$$\text{with} \quad \mathrm{k_{R1}} = 1 + \left(\frac{\mathrm{k_r}}{\mathrm{k_a}} - 1\right)\kappa_2$$

$$\text{and} \quad \kappa_2 = \frac{1}{\frac{l_{\mathrm{Fe}}}{\pi r_{\mathrm{ring}}}\frac{A_{\mathrm{ring}}}{A_{\mathrm{bar}}} Q_2 \sin^2(\pi p/Q_2) + 1},$$

where l_{Fe} is the active length of the IM, r_{ring} the middle radius and A_{ring} the area of the short circuit ring, A_{bar} the area of a rotor bar, Q_2 the number of the rotor bars and p the number of polepairs. The multiplication of the first and second time scaling factors leads to the total time scaling factor

$$\mathrm{k_t} = \mathrm{k_{t1}} \mathrm{k_{t2}}. \tag{20}$$

2) Scaling of the Winding Number: A change of the winding number in the IMs stator winding has an influence on the induced voltage and therefore on the corner speed of the IM. Therefore, the winding number is of great interest in the design of the IM espacially for a $48\,\mathrm{V}$ system. According to [12] the windingnumber is scaled with (21)-(23).

$$I \propto \frac{1}{\mathrm{k_w}} \tag{21}$$

$$\Psi \propto \mathrm{k_w} \tag{22}$$

$$L \propto \mathrm{k_w^2} \tag{23}$$

3) Scaling of the torque and losses: With the derived scaling relationships the torque and ohmic losses are scaled with (24) - (25).

$$T = \mathrm{k_a k_r^2} \tag{24}$$

$$P_{\mathrm{L,ohm,2}}^{'} = P_{\mathrm{L,ohm,2}} \mathrm{k_r^2 k_R} \tag{25}$$

The iron loss power density, separated into hysteresis, eddy current and excess losses [18] is scaled with

$$p_{\mathrm{L,Fe}}^{'} = \left(k_{\mathrm{hyst}} B^{\alpha} \frac{f}{\mathrm{k_t}} + k_{\mathrm{eddy}} B^2 \frac{f^2}{\mathrm{k_t^2}} + k_{\mathrm{excess}} B^{1.5} \frac{f^{1.5}}{\mathrm{k_t^{1.5}}}\right) \tag{26}$$

where k_{hyst}, k_{eddy} and k_{excess} are the hysteresis loss, eddy current loss and excess loss coefficient respectively. With the iron loss power density and the iron mass m_{Fe}, scaled with $\mathrm{k_r^2 k_a}$, the scaled iron loss power $P_{\mathrm{L,Fe}}^{'}$ is

$$P_{\mathrm{L,Fe}}^{'} = p_{\mathrm{L,Fe}}^{'} m_{\mathrm{Fe}} \mathrm{k_r^2 k_a}. \tag{27}$$

V. Induction Machine Optimization

The scaling laws of the IM can be used in numerical optimization procedures to achieve an optimum design of the IM. An overview of such numerical optimization procedures is presented by Stipetič and Žarko in [19]. In this publication meta-heuristic algorithm, such as Evolution Strategy or Differential Evolution, are suggested for the complex electrical machine design [20]. In [21] a multi objective optimization in combination with the scaling laws of a SM is used to find the optimum size of the traction motor as it is done in [13] with the gear ratio as an additional design variable. In this paper an Evolution Strategy is used to find the optimum design of the $48\,\mathrm{V}$ IM of the AWD vehicle. The objective parameters of the Evolution Strategy are the radial scaling factor $\mathrm{k_r}$, the axial scaling factor $\mathrm{k_a}$, the winding number w and the gear ratio i_{Gear} of the gear in the hybrid power train.

A. Objective function

The design optimization has the goal to make a chosen objective function reach its minimum or maximum value while keeping other technical indices within acceptable ranges [19]. For different field of applications different objective functions are used. Some of the typical objective functions are the minimization of the material cost or the maximization of the torque per volume [19]. In this paper the objective function is based on the equivalent fuel consumption calculation. For every operating point in the driving cycle that can be reached by the IM the equivalent consumption in this point is calculated. Here, the speed and torque dependent losses of the AWD system devices are taken into account by using the series or parallel connection of the Willans lines. With the proposed Willans approach in section III-B the equivalent consumptions in the motor and generator mode of the IM are calculated with the discharge and charge mode of the euqivalent consumption calculation procedure.

B. Reference Hybrid power train parameter

The reference hybrid power train has a gear ratio $i_{\mathrm{Gear}} = 7$, an active length of the IM $l_{\mathrm{Fe}} = 200\,\mathrm{mm}$, an outer stator radius $r_1 = 87.5\,\mathrm{mm}$, an outer rotor radius $r_2 = 51\,\mathrm{mm}$, an airgap length $l_{\mathrm{Air}} = 0.5\,\mathrm{mm}$ and a winding number $N_{\mathrm{w}} = 6$.

C. Boundary constraints

The optimization is done with certain boundary constraints. The installation space of the IM can be considered via borders of the scaling factors $\mathrm{k_r}$ and $\mathrm{k_a}$. The gear ratio i_{Gear} can also be limited by this way as well as the winding number. Further constraints in this paper are the maximum current density in the stator conductors J_{max}, the maximum surface velocity of the rotor v_{surface} and the minimum achievable torque of the hybrid power train. The constraint of the current density considers the maximum thermal stress of the stator winding concerning a maximal temperature increase of $140\,\mathrm{K}$ in $120\,\mathrm{s}$ and the maximum surface velocity of the rotor the considers the mechanical stress of the rotor. With the minimum achievable torque a costumer costumer requirement is considered. The boundary constraints for the IM in this paper are listed in table I.

	i_{Gear}	$\mathrm{k_r}$	$\mathrm{k_a}$	N_{w}	J_{max}	v_{surface}	$T_{\mathrm{axle,min}}$
min	4	0.6	0.6	1	$0\,\mathrm{A/mm^2}$	$0\,\mathrm{m/s}$	$1100\,\mathrm{N\,m}$
max	22	1.2	1.2	10	$14\,\mathrm{A/mm^2}$	$120\,\mathrm{m/s}$	∞

TABLE I
BOUNDARY CONTRAINTS OF THE IM OPTIMIZATION.

VI. SIMULATION RESULTS

To validate the proposed approach simulations are performed. With the controlled AWD model of section II-A 5 different driving cycles are simulated with different hybrid power train topologies. The simulated driving cycle are the Worldwide harmonized Light vehicles Test Procedure (WLTP), the Federal Test Procedure 75 (FTP75), the ARTEMIS Urban Cycle and the ARTEMIS Road Cycle. The simulation is done in 3 steps. First, the hybridization strategy is calculated and configured by using the equivalent fuel consumption calculation and the Willans approach describes in section III, second the optimum power train configuration is determined by using the scaling laws of the IM of section IV and by using the optimization procedure of section V. Third, the driving cycles are simulated without a hybridization, with the reference hybrid power train and with the optimized one. The vehicle is an AWD of a mass of $m_{\mathrm{Car}} = 1875\,\mathrm{kg}$, a front surface of $A = 2.61\,\mathrm{m}$, a drag force coefficient $c_{\mathrm{w}} = 0.35$ and a lifting coefficient of $c_{\mathrm{a}} = 0.2$. For a fair comparison of the difference of the SoC of the $48\,\mathrm{V}$ battery between the start and end of the drive has to be considered. By using a penalty factor in the equivalent fuel consumption minimization strategy due to Rizzoni, Pisu and Calo [22]. With this enhancement the battery SoC in the different simulations differs less than $1.2\,\%$. A further assumption in the simulation is that the ICE is completely turned off during an pure electric drive. During this situation the $12\,\mathrm{V}$ battery provides the electronic devices of the car with power. The fuel consumption difference due to a decreasing SoC of the $12\,\mathrm{V}$ battery is considered in the adjusted SoC value ΔC^*. The energy to restart the motor is not considered. Moreover, the temperature rises of the IM are neglected in a first step. The simulation results of the reference vehicle without the hybrid power train, with the reference IM with a aluminum and copper squirrel cage rotor respectively are shown in table II.

Simulation	Without IM	Ref. IM (Al)	Ref. IM (Cu)
C_{WLTP}	$6.37\,\mathrm{L}$	$-11.80\,\%$	$-12.55\,\%$
C_{FTP75}	$6.25\,\mathrm{L}$	$-16.87\,\%$	$-18.10\,\%$
$C_{\mathrm{ArtemisUrban}}$	$7.78\,\mathrm{L}$	$-24.89\,\%$	$-26.72\,\%$
$C_{\mathrm{ArtemisRoad}}$	$5.78\,\mathrm{L}$	$-9.97\,\%$	$-10.34\,\%$

TABLE II
RESULTS OF THE IM OPTIMIZATION AND VEHICLE SIMULATION (ALUMINUM CAGE).

The results of the IM optimization are listed in table III. It shows the optimum gear ratio, radial and axial scaling factor and winding number of the IM. The consumption difference ΔC^* and the adjusted consumption difference ΔC^* show that the optimized motor design results in a fuel consumption saving of $2.3\,\%$ to $7.4\,\%$ depending on the driving cylce. It also shows that the optimum gear ratio is in the range of 9, the optimum radial scaling factor 1.17, the optimum axial scaling factor in the range of 0.9 and the winding number 3 or 4.

Driving Cycle	i_{Gear}	$\mathrm{k_r}$	$\mathrm{k_a}$	N_{w}	ΔC	ΔC^*
WLTP	9.6645	1.1771	0.9952	3	$-14.14\,\%$	$-13.95\,\%$
FTP 75	8.6945	1.1788	0.8878	4	$-22.46\,\%$	$-22.26\,\%$
Artemis Urban	9.8726	1.1802	1.200	4	$-34.36\,\%$	$-34.26\,\%$
Artemis Road	9.6712	1.1828	0.9488	3	$-12.77\,\%$	$-12.68\,\%$

TABLE III
RESULTS OF THE IM OPTIMIZATION AND VEHICLE SIMULATION (ALUMINUM CAGE).

Driving Cycle	i_{Gear}	$\mathrm{k_r}$	$\mathrm{k_a}$	N_{w}	ΔC	ΔC^*
WLTP	8.2088	1.1917	0.994	3	$-15.04\,\%$	$-14.86\,\%$
FTP 75	8 2456	1.1875	0.8561	4	$-23.06\,\%$	$22.86\,\%$
Artemis Urban	6.1642	1.1896	1.1904	4	$-34.96\,\%$	$-34.87\,\%$
Artemis Road	9.7661	1.1949	1.0409	3	$-13.37\,\%$	$-13.27\,\%$

TABLE IV
RESULTS OF THE IM OPTIMIZATION AND VEHICLE SIMULATION (COPPER CAGE).

Table IV shows the results of a copper squirrel cage induction machine. The results indicate that for this type of IM the gear ratio is less than for the aluminum version and the consumption savings are up to $0.9\,\%$ higher. The optimization and simulation results show that a high diameter of the IM has a more important influence on the fuel consumption savings potential than its length. It also indicates that the machine's size as an optimum value below the maximum allowed dimensions. The fact that the optimum gear ratio is, in this driving cycles and vehicle configuration, in the range of 9 is an interesting information for the machine design.

VII. CONCLUSIONS AND FUTURE WORK

In this paper an optimization approach of an $48\,\mathrm{V}$ IM in a hybrid vehicle is proposed. The procedure consists of several parts. With the equivalent fuel consumption calculation and the Willans approach a hybrid strategy is defined. Furtermore, it is used to define the objective function of an Evolutionary Strategy that optimized the gear ratio, the radial and axial length and the winding number of the used $48\,\mathrm{V}$ IM. For the Evolutionary Strategy scaling laws of IM are taken into account. The optimization considers different boundary constraints such as a maximum rotor surface velocity, a minimum achievable pure electric torque or a maximum current density in the stator windings. The reference and optimized machine designs are simulated by a vehicle model with using different driving cycles. The simulation results show that the procedure is able to find an optimum machine size and gear ration which reduces the fuel consumption significantly, compared to the reference machine. In future work a more detailed description of the scaling laws of IMs will be proposed. Besides the radial and axial scaling the scaling laws description will also consider the change of the rotor bar conductivity due to material or temperature variations. Other future work will focus on the improvement of the proposed optimization procedure and the hybrid vehicle simulation. The temperature changes of the IM during its operation will be considered as well as more boundary constraints and parameter in the optimization algorithm.

REFERENCES

[1] E. Silvas, T. Hofman, N. Murgovski, L. F. P. Etman, and M. Steinbuch, "Review of optimization strategies for system-level design in hybrid electric vehicles," *IEEE Transactions on Vehicular Technology*, vol. 66, no. 1, pp. 57–70, 1 2017.

[2] G. Paganelli, S. Delprat, T. M. Guerra, J. Rimaux, and J. J. Santin, "Equivalent consumption minimization strategy for parallel hybrid powertrains," *Vehicular Technology Conference. IEEE 55th Vehicular Technology Conference. VTC*, vol. 4, pp. 2076–2081, 2002.

[3] K. Rhode-Brandenburger, *Bewertungsansätze zu Verbrauch und Fahrleistung*. In: Energiemanagement in Kraftfahrzeugen, ATZ/MTZ-Fachbuch, Springer Vieweg, Wiesbaden, 2014.

[4] C. Desai and S. S. Williamson, "Comparative study of hybrid electric vehicle control strategies for improved drivetrain efficiency analysis," *IEEE Electrical Power & Energy Conference (EPEC), Montreal, QC*, pp. 1–6, 2009.

[5] Y. Li and B. Chen, "Development of integrated rule-based control and equivalent consumption minimization strategy for hev energy management," *12th IEEE/ASME International Conference on Mechatronic and Embedded Systems and Applications (MESA), Auckland*, pp. 1–6, 2016.

[6] D. D. R, M. Morandin, S. Bolognani, and M. Castiello, "A threshold logic control strategy for parallel light hybrid electric vehicle implementation," *8th IET International Conference on Power Electronics, Machines and Drives (PEMD 2016), Glasgow*.

[7] E. Vinot, R. Trigui, B. Jeanneret, J. Scordia, and F. Badin, "Hevs comparison and components sizing using dynamic programming," *IEEE Vehicle Power and Propulsion Conference, Arlington, TX*, pp. 314–321, 2007.

[8] F. Zhang, J. Xi, and R. Langari, "An adaptive equivalent consumption minimization strategy for parallel hybrid electric vehicle based on fuzzy pi," *IEEE Intelligent Vehicles Symposium (IV), Gothenburg*, pp. 460–465, 2016.

[9] G. von Pfingsten, M. Nell, and K. Hameyer, "Hybrid simulation methods for induction machine calculation reduction of simulation effort by coupling static fea with transient fea and analytic formulations," in *2017 18th International Symposium on Electromagnetic Fields in Mechatronics, Electrical and Electronic Engineering (ISEF) Book of Abstracts*, Sept 2017, pp. 1–2.

[10] G. von Pfingsten and K. Hameyer, "Highly efficient approach to the simulation of variable-speed induction motor drives," *IET Science, Measurement Technology*, vol. 11, no. 6, pp. 793–801, 2017.

[11] S. Stipetič, D. Žarko, and M. Popescu, "Scaling laws for synchronous permanent magnet machines," in *2015 Tenth International Conference on Ecological Vehicles and Renewable Energies (EVER)*, March 2015, pp. 1–7.

[12] ——, "Ultra-fast axial and radial scaling of synchronous permanent magnet machines," *IET Electric Power Applications*, vol. 10, no. 7, pp. 658–666, 2016.

[13] K. Ramakrishnan, S. Stipetič, M. Gobbi, and G. Mastinu, "Multi-objective optimization of electric vehicle powertrain using scalable saturated motor model," in *2016 Eleventh International Conference on Ecological Vehicles and Renewable Energies (EVER)*, April 2016, pp. 1–6.

[14] D. Žarko, M. Kovačić, S. Stipetič, and D. Vuljaj, "Optimization of electric drives for traction applications," in *2017 19th International Conference on Electrical Drives and Power Electronics (EDPE)*, Oct 2017, pp. 15–32.

[15] D. ZARKO, "Design of premium efficiency (ie3) induction motors using evolutionary optimization and scaling laws," vol. 1, pp. 183–186, 12 2016.

[16] J. C. H. Bone, "Influence of rotor diameter and length on the rating of induction motors," *Electric Power Applications, IEE Journal on*, vol. 1, no. 1, pp. 2–6, February 1978.

[17] K. T. Hsieh and B. K. Kim, "One kind of scaling relations on electromechanical systems," *IEEE Transactions on Magnetics*, vol. 33, no. 1, pp. 240–244, Jan 1997.

[18] G. von Pfingsten, S. Steentjes, and K. Hameyer, "Transient approach to model operating point dependent losses in saturated induction machines," in *2016 XXII International Conference on Electrical Machines (ICEM)*, Sept 2016, pp. 626–632.

[19] S. Stipetič, W. Miebach, and D. Žarko, "Optimization in design of electric machines: Methodology and workflow," in *2015 Intl Aegean Conference on Electrical Machines Power Electronics (ACEMP), 2015 Intl Conference on Optimization of Electrical Electronic Equipment (OPTIM) 2015 Intl Symposium on Advanced Electromechanical Motion Systems (ELECTROMOTION)*, Sept 2015, pp. 441–448.

[20] K. Hameyer and R. Belmans, *Numerical Modelling and Design of Electrical Machines and Devices*, ser. Advances in electrical and electronic engineering. WIT Press, 1999.

[21] K. Ramakrishnan, S. Stipetič, M. Gobbi, and G. Mastinu, "Optimal sizing of traction motors using scalable electric machine model," *IEEE Transactions on Transportation Electrification*, vol. PP, no. 99, pp. 1–1, 2017.

[22] G. Rizzoni, P. Pisu, and E. Calo, "Control strategies for parallel hybrid electric vehicles," *IFAC Proceedings Volumes*, vol. 37, no. 22, pp. 495 – 500, 2004.